ACS APPLIED MATERIALS & INTERFACES

Letter

Cite This: ACS Appl. Mater. Interfaces 2018, 10, 34811−34816

www.acsami.org

Single-Cell Tumbling Enables High-Resolution Size Profiling of Retinal Stem Cells

Surath Gomis,[†] Mahmoud Labib,[‡] Brenda L. K. Coles,[§] Derek van der Kooy,*[,§] Edward H. Sargent,*[,†] and Shana O. Kelley*[,‡]

[†]Department of Electrical and Computer Engineering, University of Toronto, Toronto, Ontario M5S 3G4, Canada

[‡]Department of Pharmaceutical Sciences, University of Toronto, Toronto, Ontario M5S 3M2, Canada

[§]Department of Molecular Genetics, University of Toronto, Toronto, Ontario M5S 1A8, Canada

Supporting Information

ABSTRACT: Retinal stem cells (RSCs) are promising candidates for patient-derived cell therapy to repair damage to the eye; however, RSCs are rare in retinal samples and lack validated markers, making cell sorting a significant challenge. Here we report a high-resolution deterministic lateral displacement microfluidic device that profiles RSCs in distinct size populations. Only by developing a chip that promotes cell tumbling do we limit cell deformation through apertured channels and thereby increase the size-sorting resolution of the device. We systematically explore a spectrum of microstructures, including optimized notched pillars, to study and then rationally promote cell tumbling. We find that RSCs exhibit larger diameters than most ciliary epithelial cells, an insight into RSC morphology that allows enrichment from biological samples.

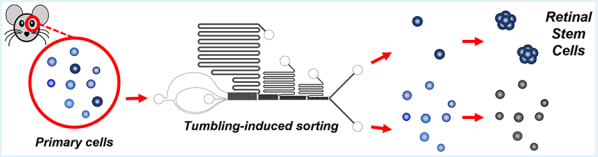

KEYWORDS: *retinal stem cells, microfluidics, deterministic lateral displacement, ciliary epithelium, label-free, size-sorting, cell tumbling*

The degeneration of cones and rods, the photoreceptive cells of the retina, is the leading cause of vision loss in the developed world and manifests itself in diseases such as age-related macular degeneration.[1] Although some treatments can slow retinal degeneration by replenishing the layer of retinal pigmented epithelium (RPE) that support photoreceptors,[2−4] the regeneration of both RPE and photoreceptors is necessary to reverse retinal degeneration, i.e., reverse blindness.

Retinal stem cells (RSCs) are a promising candidate for reversing retinal degeneration because RSCs are multipotential adult stem cells found in the ciliary epithelium (CE) at the retinal periphery of the mammalian eye,[5] as depicted in Figure 1a. Although these cells help to build the retina in the embryo, in the adult they are quiescent in vivo. RSCs have been demonstrated to differentiate into all retinal cell types of the neural retina and the retinal pigmented epithelium in vitro and demonstrate self-renewal upon passaging.[5,6] The fact that RSCs are stem cells found in adults makes them appealing targets as they could be patient-derived for therapeutic applications, limiting rejection, tumorigenic issues, and potential ethical issues associated with many other stem cell therapies such as those derived from embryonic stem cells.

A major challenge that hinders the study of RSCs, however, is that they are an extremely rare cell type, and this fact has limited their characterization. Previous studies have isolated RSCs based on P-cadherin expression, but the fact that this marker has low expression levels limited the enrichment to ∼0.2% when conventional fluorescence-activated cell sorting (FACS) was used for cell isolation.[7] Moreover, under 10% cell recovery was observed due to cell death during sorting.

We hypothesized that a microfluidic approach could provide a compelling new solution for RSC isolation as microfluidic devices can enable highly specific characterization of a variety of biological samples.[8−11] For RSCs, both the rarity of these cells and the lack of unique surface markers necessitated the development of a microfluidic approach which can be sensitive to low cell numbers, sort live cells and maintain viability, and do so without the use of labels given the lack of information regarding surface expression on these cells.

Many label-free microfluidic techniques can be applied to cell sorting,[12,13] using characteristics such as size, shape, density, and deformability, and sorting principles that manipulate flow using microstructures,[14] inertial effects,[15] gravity,[16] centrifugation,[17] and electrical properties of cells.[18] We identified size-based sorting as the most practical modality for our RSC study as qualitative information from the literature indicates that RSCs may be the larger pigmented cells of the CE.[7]

However, to conduct a quantitative size-based profiling of RSCs for the first time, we needed first to improve upon the sorting resolution achieved with previous devices. Specifically, we sought to produce devices that segregate well-defined subpopulations of cells with minimal overlap. In contrast to the

Received: June 24, 2018
Accepted: September 28, 2018
Published: September 28, 2018

DOI: 10.1021/acsami.8b10513
ACS Appl. Mater. Interfaces 2018, 10, 34811−34816

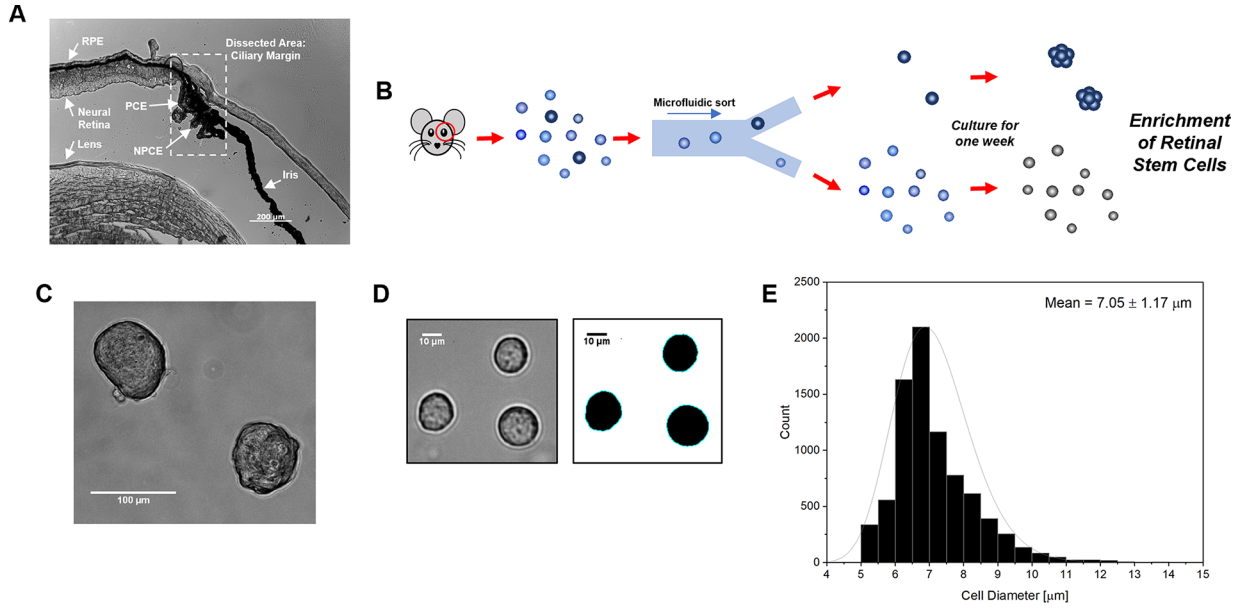

Figure 1. Retinal stem cells are a rare cell type harvested from a heterogeneous collection of ciliary epithelial cells. (A) Cross-section of a mouse eye showing the ciliary epithelium (CE), with both the pigmented ciliary epithelium (PCE) and nonpigmented ciliary epithelium (NPCE) components shown. The CE is contiguous with the retinal pigmented epithelium (RPE). The eye of a pigmented animal is shown to more easily distinguish cell layers. (B) Primary cells are dissected from the CE of a mouse eye. Our device is then used to sort RSCs based on size. A sphere forming assay is performed on all outlet populations by plating them in nonadherent cell culture conditions for 1 week, where only the RSCs will proliferate into a spherical colony. (C) Retinal stem cells that have proliferated into spherical colonies after a week in nonadherent cell culture, where one sphere correlates to the existence of one RSC. (D) Bright-field imaging was used to image CE cells and extract size data by batch processing images using ImageJ software. (E) Cell size distribution from the mouse ciliary epithelium. The distribution is slightly left skewed and fits within a normal distribution of cells with diameters between ∼5−10 μm.

case of sorting solid spherical particles (e.g., polystyrene beads) often used in characterizing size-sorting devices,[14] the sorting of soft particles like cells suffers the effects of deformation under fluid flow. This, we show herein, is directly responsible for unpredictable trajectories and low-resolution sorting, requiring advancements in microfluidic size-sorting techniques to correctly profile RSCs.

We describe a microfluidic size-based sorter utilizing notched microstructures for deterministic lateral displacement (DLD) that promotes single-cell tumbling to effectively sort RSCs. We induce tumbling to increase sorting resolution by reducing cell deformability during passage through the device. The new device is designed to sort cells into five distinct size-based populations, where notched microstructures best enhanced the distinction between size-populations compared to other tested structures, including standard circular pillars. By using our device, we have determined the cell size to target to yield the highest RSC enrichment.

The strategy behind our label-free microfluidic RSC sort is outlined in Figure 1b. A primary cell sample is obtained by dissecting the ciliary epithelium of adult albino CD1 mouse eyes and is then processed through our device. The primary cells found in the dissected region of the eye include RSCs, retinal pigmented epithelial cells, red blood cells, and muscle cells. To determine the existence of RSCs in the outlet samples, they are propagated at low densities using non-adherent cell culture conditions, namely a clonal sphere-forming assay, for 1 week.[5,6] During this period, the proliferative RSCs form large (>75 μm) spherical colonies, where one sphere is produced clonally by the proliferation of one RSC[5,7] (Figure 1c).

To identify the size-sorting criteria for our device, we needed first to profile the size distribution of the primary CE population. This was achieved by imaging multiple CE cell samples using brightfield microscopy, ensuring the cell membranes were distinguishable to realize the full cell size (Figure 1d). ImageJ software was then used to batch process calculations of cell diameter, generating the distribution illustrated in Figure 1e. This initial screening demonstrates that the population of cells derived from the CE have diameters within a small window of ∼5−10 μm. Current approaches to size-based sorting cannot easily distinguish between cells which differ in this range, with the majority of size-sorting microfluidic devices being used to sort cells from uniquely shaped red blood cells.[13,19] This made it necessary for us to design a high-resolution microfluidic sorter in order to profile RSCs.

We proceeded to design a separation device based on deterministic lateral displacement (DLD), a size-based sorting technique which was first used to distinguish solid spherical particles with a designed critical diameter.[14] DLD devices use offset rows of pillars within a microfluidic channel which repeat at a specified periodicity. This pattern causes fluid to form multiple, periodic streamlines of known trajectories, where particles larger than the critical diameter are laterally displaced, i.e., are shuttled diagonally between streamlines, and particles smaller than the critical diameter stay within a single streamline in a net straight trajectory through the channel, leading to particle fractionation. Our device was designed to enhance the cell-sorting resolution achievable with DLD by (i) taking advantage of multiple DLD array regions, and (ii) incorporating structures promoting cell tumbling.

DOI: 10.1021/acsami.8b10513
ACS Appl. Mater. Interfaces 2018, 10, 34811−34816

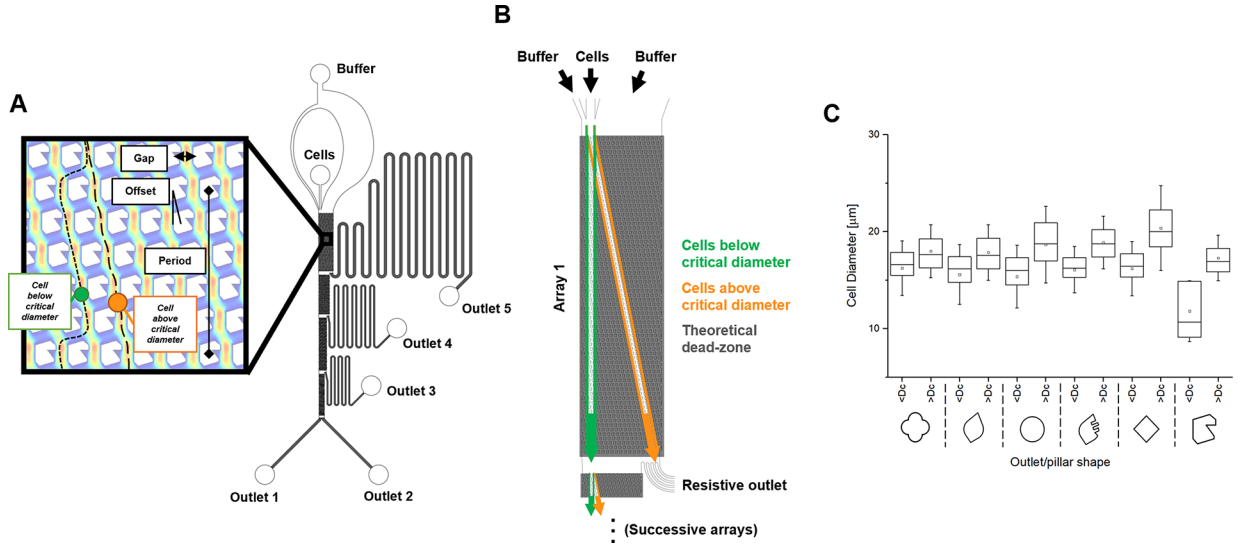

Figure 2. Device for high resolution size-based cell profiling and sorting performance data. (A) Deterministic lateral displacement (DLD) is a passive size-based sorting technique which uses offset arrays of posts with a designed periodicity between rows to sort cells above and below a designed critical diameter. A cascading DLD design with four active regions and five outlets to sort cells is used to characterize the size distribution of RSCs in five size populations. The velocity surface of the inset was generated using COMSOL Multiphysics. (B) Device design considerations to improve sorting resolution include a wide theoretical cell fractioning with wide and long post arrays to introduce sorting corrections through redundancy, and buffer flow along outer walls to eliminate edge effects. Outlet resistances were calculated to ensure vertical flow. (C) Repeated tests were conducted using six different pillar shapes in binary DLD devices to test the effects of triangular and tumbling structures at an inlet flow rate of 20 μL/min. Each device has an outlet with cells less than the critical diameter ($<D_c$) and greater than the critical diameter ($>D_c$). The notched pillar shape performed the best, fractioning the inlet LNCaP cell population into two distinct populations with a minimal 10% overlap.

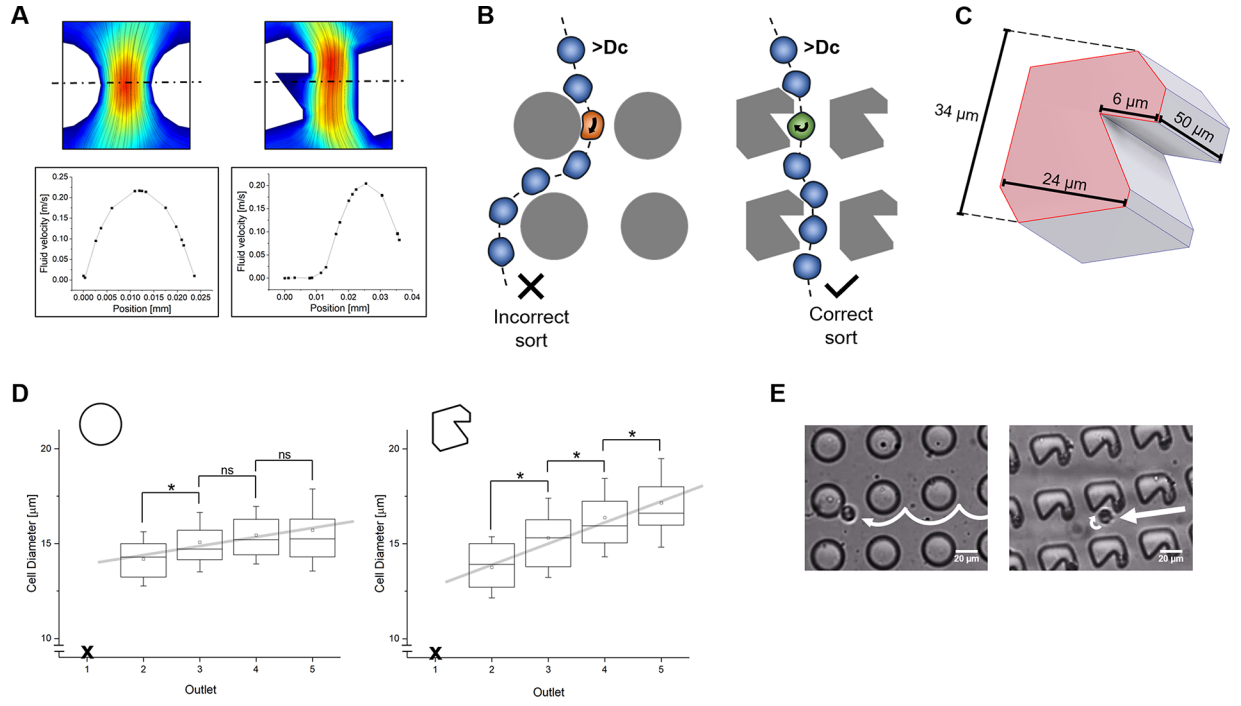

Figure 3. Notched microstructures improve the resolution of cell sorting. (A) The notched microstructure, compared to circular pillars, has a near zero velocity zone in its void, which allows a cell to rotate as it experiences shear stress. A velocity field slice is shown between gaps of both pillars for an inlet flow rate of 5 μL/min. The velocity profiles were generated using COMSOL Multiphysics. (B) Cells deform as they hit circular pillars, decreasing their effective size such that they act as smaller particles upon sort. Using notched microstructures, the void allows the cell to rotate and retain its sphericity to sort correctly. (C) Dimensions of the notched microstructure. (D) Performance of standard circular pillars versus notched microstructures in the fully realized five-outlet sorter, having sorted LNCaP cells at an inlet flow rate of 20 μL/min. The notched microstructures have superior sorting resolution, with all populations having distinct means ($p < 0.05$) compared to the circular pillars. A random sampling of 50 cells per outlet were measured from brightfield microscope scans to recover cell size data. (E) Experimental depiction of cell tumbling as a cell interrogates notched microstructures and circular pillars. Rather than hitting pillars and sliding off in a cycloid motion when interrogating circular pillars, causing cell deformation, cells moving around the notched microstructures rotate and follow a straight trajectory.

DOI: 10.1021/acsami.8b10513
ACS Appl. Mater. Interfaces 2018, 10, 34811−34816

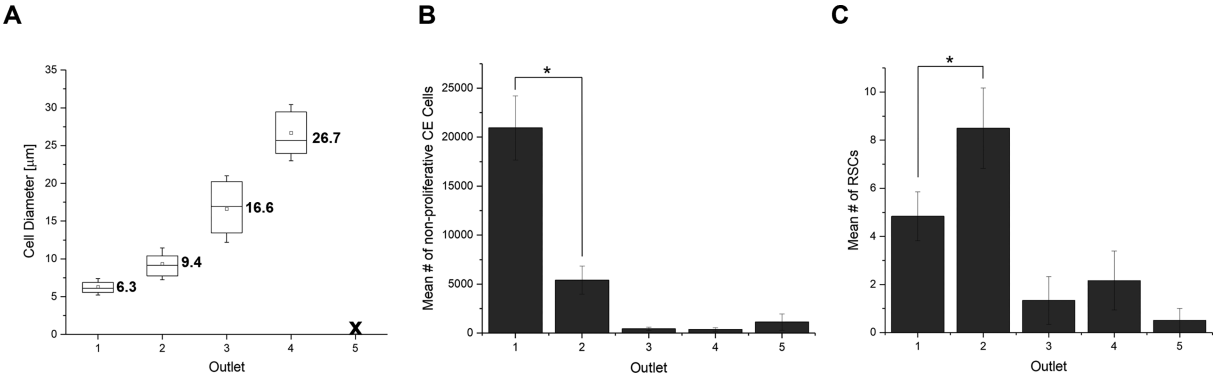

Figure 4. Retinal stem cells isolated based on size. (A) Size ranges of the outlet populations upon a CE cell sort using our fully realized five-outlet notched DLD device, at an inlet flow rate of 5 μL/min. Each outlet population has a distinct mean size in micrometers as shown ($p < 0.05$). A random sampling of 1500 cells were measured from bright-field microscopy scans to recover cell size data. (B) The majority of nonproliferative CE cells are sorted into Outlet 1, determined to have a mean diameter of 6.3 ± 1.1 μm. (C) Majority of RSCs sorted into Outlet 2, determined to have a mean diameter of 9.4 ± 2.1 μm. We demonstrate the depletion of the majority of nonproliferative CE cells via sorting into Outlet 1 while most RSCs sorted into Outlet 2. The RSC count in Outlet 2 is significantly larger than the count in Outlet 1 ($p < 0.05$) using a two-sample t test after confirming distribution normality, and the counts in Outlets 3, 4, and 5 are not significantly different than zero using one sample t tests. Standard error of the mean is shown for panels b and c.

To permit size profiling using DLD, our device implements four DLD arrays with successively smaller critical diameters such that cells can be fractioned into five population outlets (Figure 2a). In prior work, this cascading technique was used primarily as a filtration technique to reduce clogging from larger cells,[19] however here we use it to profile a single cell type. The resistances of outlet channels were calculated to maintain a straight velocity profile through the interface between successive DLD arrays, modeled using a resistive circuit analogy,[20] and optimized using COMSOL Multiphysics. The cell and buffer inlet widths were designed to focus the cell inlet stream, and buffer flowing on both sides of the cell inlet minimizes cell interactions with the walls. The device widths in each array section were designed such that the theoretical cell paths are spaced by large dead zones as margins for sorting error corrections (Figure 2b).

To achieve the sorting resolution necessary to distinguish particles within the 5 μm size distribution of CE cells, we designed and tested a variety of pillar shapes to promote cell tumbling. Our pillar design effort examined the properties of triangular pillars,[21] I-shaped pillars,[22] and asymmetric pillars previously used for the sorting of CTC clusters.[23] We conducted these studies by fabricating six binary sorting DLD devices, i.e. devices which sort about a single critical diameter, with only the pillar shapes differing between each design. We designed the devices to sort about a theoretical 12 μm critical diameter (Dc) based on the empirical formula used for circular pillar arrays[20] and conducted a repeated experiment using LNCaP cells, a readily available epithelial cell line. The six pillar shapes tested include the circle (as reference), flower (circle-like with tumbling protrusions), diamond and leaf (triangular-like without tumbling protrusions), and rough leaf and notched (triangular-like with tumbling protrusions).

The results of our pillar shape analysis are depicted in Figure 2c. Sorting resolution was evaluated by measuring the extent of overlap between the two outlet populations. We extracted a quantitative measurement using a distribution overlapping coefficient (OVL), representing the percentage distribution overlap,[24] to compare each device to one another. Overall, we found that pillars with both tumbling and triangular-like features outperformed those without. In particular, the notched microstructure performed the best by having the clearest distinction between outlet populations (OVL = 0.1, compared to OVL = 0.4 for circular posts). Furthermore, unlike the other shapes, including the diamond (OVL = 0.2), the notched microstructure led to size fractionation occurring closest to the theoretical critical diameter.

The performance of the notched microstructures suggests that cells are indeed tumbling with limited cell deformability to increase the resolution of sorting. We correlate limited deformability with the decreased overlap of outlet population sizes in our device. The principle behind tumbling in the notched microstructures is that they induce constant single cell rotation under fluid flow, allowing cells to maintain their average static spherical diameter when interrogating pillars. The rotation is possible because of the near-zero velocity field within the notch, creating a void where a cell experiences shear stress on the order of the wall shear stress it would feel pressed against a pillar, but now with space to freely tumble (Figure 3a). In contrast, in the absence of tumbling such as in a DLD device with circular pillars, if the particle to be sorted has a diameter larger than the critical diameter but is deformable, collisions with posts will decrease the effective size of the cell and lead it to be incorrectly sorted as a smaller particle[25] (Figure 3b). It has been suggested that protrusions in pillars, a defining feature of our notched microstructures, cause inertial effects in the cells—effects that are generally ignored in DLD devices—with lateral perturbations in momentum to increase separation efficiency.[26] The effects of deformation on sorting resolution is also a function of fluid velocity and pillar size, where an increase in either parameter reduces sorting resolution due to increased shear stress and collisions.[25,27] Additional features of our notch include the void having a depth on the order of average CE cell size to ensure the cell experiences the velocity gradient. The notch also tapers downward to avoid cell capture and the pillars are pointed in the direction of fluid flow on the premise of reduced clogging.[21] Device dimensions are outlined in Figure 3c. Optimizations of device geometries and fluid flow rates were performed, and the results are included in the Supporting Information. It was found that flow rates of 5−20 μL/min and

DOI: 10.1021/acsami.8b10513
ACS Appl. Mater. Interfaces 2018, 10, 34811−34816

high pillar aspect ratios were the most suitable for our RSC study.

We further demonstrated that our notched microstructures have similar performance when used in a device featuring multiple DLD arrays. Using LNCaP cells, we compared the performance of the notched structures and circular pillars in five-outlet devices. These results are depicted in Figure 3d, where the LNCaP cells were sorted into the four larger outlets of the devices, but only in the notched microstructure device are the four population means significantly different from one another ($p < 0.05$). This experiment is particularly illuminating because LNCaP is a single, homogeneous cell line, demonstrating the high-resolution sorting capabilities of our notched microstructures relative to circular pillars. Furthermore, cell viability after the experiment was 80%, and cell recovery (i.e., the ratio of cells entering to cells exiting the device) was 80% in our notched microstructure device. We can visualize the notched microstructure performance by examining fluidic channels under a microscope, where while a cell moving through a circular pillar array will move in a cycloid pattern as it collides with pillars, a cell moving through the notched pillar array maintains a straight trajectory and continuously rotates within the notched regions (Figure 3e).

Using this five-outlet notched DLD device, we profiled the size distribution of RSCs to determine whether RSCs could be distinguished from the other cells of the CE. Small cell samples from each device outlet were used for brightfield imaging of the cells to associate each outlet with the cell size range that was sorted. We found that the majority of the sorted CE population was fractioned into Outlet 1 (mean cell diameter = 6.3 ± 1.1 μm) and Outlet 2 (mean cell diameter = 9.4 ± 2.1 μm), with Outlet 3 and 4 containing few cell clusters, and Outlet 5 having too few cells to count (Figure 4a). Our device performed very well sorting CE cells as each of the populations had both distinct means ($p < 0.05$) and minimal distribution overlaps between each outlet (OVL = 0.2 between Outlet 1 and Outlet 2).

We then conducted a CE cell sort using our device to enrich the RSC population. We first counted the sorted CE cells using a hemocytometer directly after processing cells through our device, and collected RSC counts a week later after conducting a sphere forming assay. We found that that while the majority of nonproliferative CE cells collected in Outlet 1 with mean diameters of 6.3 ± 1.1 μm, the majority of RSCs were collected in Outlet 2 with mean diameters of 9.4 ± 2.1 μm. The counts for nonproliferative CE cells and RSCs are depicted in Figure 4b, c, respectively. Furthermore, the RSC count in Outlet 2 is significantly larger than the count in Outlet 1 ($p < 0.05$, $N = 6$) and the RSC counts in Outlets 3 to 5 are not significantly larger than zero (Figure 4c).

We have demonstrated that the majority of RSCs exist as larger cells within the CE and have determined that their sizes to fall within the range 9.4 ± 2.1 μm. Furthermore, we have demonstrated a major depletion of nonproliferative CE cells from the RSC population due to the sorting of these cells into Outlet 1. Although the enrichment of the RSC population in Outlet 2 is still low, ~0.5%, this is over a 2-fold increase in enrichment compared to that obtained using FACS. Furthermore, our method maintains high cell recovery upward of 80%, compared to the 10% from FACS.

In sum, we have profiled RSCs based on their size by designing a high-resolution size-based sorting microfluidic device. By utilizing notched microstructures arrayed for deterministic lateral displacement, we have separated primary CE cells into distinct size populations and have found that the majority of RSCs exist within an enriched population of cells with diameter 9.4 ± 2.1 μm. Our technique improves RSC enrichment and viability compared to conventional FACS. Our sorting device can be used as an enrichment step for future RSC genetic sequencing in order to discover unique RSC markers. Owing to the high-resolution sorting capabilities of our notched microstructure DLD device, this investigation of RSCs has given us some of the first quantitative measures of morphological characteristics to probe for in future RSC studies.

■ ASSOCIATED CONTENT

Supporting Information

The Supporting Information is available free of charge on the ACS Publications website at DOI: 10.1021/acsami.8b10513.

Device design; methods for device fabrication; methods for processing cells; methods for cell counting; optimization results for inlet flow rates; optimization results for pillar diameter; image of the fabricated five-outlet notched DLD device; binary DLD device schematic; dimensions of fabricated five-outlet notched DLD device; overlapping coefficients of the outlet populations of the six pillar shapes; overlapping coefficients of the RSC outlet populations; mean cell diameter and standard deviations for RSC outlet populations; description of microscope video of the device with circular pillars in operation; description of microscope video of the device with notched microstructures in operation (PDF)

Video S1, device with circular pillars in operation (MPG)

Video S2, device with notched microstructures in operation (MPG)

■ AUTHOR INFORMATION

Corresponding Authors

*E-mail: shana.kelley@utoronto.ca.
*E-mail: ted.sargent@utoronto.ca.
*E-mail: derek.van.der.kooy@utoronto.ca.

ORCID

Edward H. Sargent: 0000-0003-0396-6495
Shana O. Kelley: 0000-0003-3360-5359

Author Contributions

S.G. conceived and designed devices, experiments, and aided with manuscript writing. M.L. and B.L.K.C. aided in conducting experiments and analyzing data. S.O.K., E.H.S., and D.V.D.K. supervised the study and aided in project guidance. All authors contributed to editing and approval of the final version of the manuscript.

Notes

The authors declare no competing financial interest.

■ ACKNOWLEDGMENTS

This research was undertaken thanks to funding from the Canadian Institutes of Health Research (FDN-148415) and the University of Toronto's Medicine by Design initiative, which receives funding from the Canada First Research Excellence Fund (CFREF).

DOI: 10.1021/acsami.8b10513
ACS Appl. Mater. Interfaces 2018, 10, 34811−34816

REFERENCES

(1) Bourne, R. R. A.; Jonas, J. B.; Flaxman, S. R.; Keeffe, J.; Leasher, J.; Naidoo, K.; Parodi, M. B.; Pesudovs, K.; Price, H.; White, R. A.; Wong, T. Y.; Resnikoff, S.; Taylor, H. R. Prevalence and Causes of Vision Loss in High-Income Countries and in Eastern and Central Europe: 1990−2010. *Br. J. Ophthalmol.* **2014**, *98*, 629−638.

(2) Schwartz, S. D.; Hubschman, J.-P.; Heilwell, G.; Franco-Cardenas, V.; Pan, C. K.; Ostrick, R. M.; Mickunas, E.; Gay, R.; Klimanskaya, I.; Lanza, R. Embryonic Stem Cell Trials for Macular Degeneration: A Preliminary Report. *Lancet* **2012**, *379*, 713−720.

(3) Da Cruz, L.; Fynes, K.; Georgiadis, O.; Kerby, J.; Luo, Y. H.; Ahmado, A.; Vernon, A.; Daniels, J. T.; Nommiste, B.; Hasan, S. M.; Gooljar, S. B.; Carr, A. F.; Vugler, A.; Ramsden, C. M.; Bictash, M.; Fenster, M.; Steer, J.; Harbinson, T.; Wilbrey, A.; Tufail, A.; Feng, G.; Whitlock, M.; Robson, A. G.; Holder, G. E.; Sagoo, M. S.; Loudon, P. T.; Whiting, P.; Coffey, P. J. Phase 1 Clinical Study of an Embryonic Stem Cell-Derived Retinal Pigment Epithelium Patch in Age-Related Macular Degeneration. *Nat. Biotechnol.* **2018**, *36*, 328−337.

(4) Mehat, M. S.; Sundaram, V.; Ripamonti, C.; Robson, A. G.; Smith, A. J.; Borooah, S.; Robinson, M.; Rosenthal, A. N.; Innes, W.; Weleber, R. G.; Lee, R. W. J.; Crossland, M.; Rubin, G. S.; Dhillon, B.; Steel, D. H. W.; Anglade, E.; Lanza, R. P.; Ali, R. R.; Michaelides, M.; Bainbridge, J. W. B. Transplantation of Human Embryonic Stem Cell-Derived Retinal Pigment Epithelial Cells in Macular Degeneration. *Ophthalmology* **2018**, 1−11.

(5) Tropepe, V.; Coles, B. L.; Chiasson, B. J.; Horsford, D. J.; Elia, A. J.; McInnes, R. R.; van der Kooy, D. Retinal Stem Cells in the Adult Mammalian Eye. *Science* **2000**, *287*, 2032−2036.

(6) Ahmad, I.; Tang, L.; Pham, H. Identification of Neural Progenitors in the Adult Mammalian Eye. *Biochem. Biophys. Res. Commun.* **2000**, *270*, 517−521.

(7) Ballios, B. G.; Clarke, L.; Coles, B. L. K.; Shoichet, M. S.; van Der Kooy, D. The Adult Retinal Stem Cell Is a Rare Cell in the Ciliary Epithelium Whose Progeny Can Differentiate into Photoreceptors. *Biol. Open* **2012**, *1*, 237−246.

(8) Nourmohammadzadeh, M.; Xing, Y.; Lee, J. W.; Bochenek, M. A.; Mendoza-Elias, J. E.; McGarrigle, J. J.; Marchese, E.; Chun-Chieh, Y.; Eddington, D. T.; Oberholzer, J.; Wang, Y. A Microfluidic Array for Real-Time Live-Cell Imaging of Human and Rodent Pancreatic Islets. *Lab Chip* **2016**, *16*, 1466−1472.

(9) Kang, D.-K.; Ali, M. M.; Zhang, K.; Huang, S. S.; Peterson, E.; Digman, M. A.; Gratton, E.; Zhao, W. Rapid Detection of Single Bacteria in Unprocessed Blood Using Integrated Comprehensive Droplet Digital Detection. *Nat. Commun.* **2014**, *5*, 5427.

(10) Yesiloz, G.; Boybay, M. S.; Ren, C. L. Label-Free High-Throughput Detection and Content Sensing of Individual Droplets in Microfluidic Systems. *Lab Chip* **2015**, *15*, 4008−4019.

(11) Loring, J. F.; McDevitt, T. C.; Palecek, S. P.; Schaffer, D. V.; Zandstra, P. W.; Nerem, R. M. A Global Assessment of Stem Cell Engineering. *Tissue Eng., Part A* **2014**, *20*, 2575−2589.

(12) Gossett, D. R.; Weaver, W. M.; Mach, A. J.; Hur, S. C.; Tse, H. T. K.; Lee, W.; Amini, H.; Di Carlo, D. Label-Free Cell Separation and Sorting in Microfluidic Systems. *Anal. Bioanal. Chem.* **2010**, *397*, 3249−3267.

(13) Wyatt Shields IV, C.; Reyes, C. D.; López, G. P. Microfluidic Cell Sorting: A Review of the Advances in the Separation of Cells from Debulking to Rare Cell Isolation. *Lab Chip* **2015**, *15*, 1230−1249.

(14) Huang, L. R.; Cox, E. C.; Austin, R. H.; Sturm, J. C. Continuous Particle Separation through Deterministic Lateral Displacement. *Science* **2004**, *304*, 987−990.

(15) Di Carlo, D. Inertial Microfluidics. *Lab Chip* **2009**, *9*, 3038.

(16) Huh, D.; Bahng, J. H.; Ling, Y.; Wei, H. H.; Kripfgans, O. D.; Fowlkes, J. B.; Grotberg, J. B.; Takayama, S. Gravity-Driven Microfluidic Particle Sorting Device with Hydrodynamic Separation Amplification. *Anal. Chem.* **2007**, *79*, 1369−1376.

(17) Yu, Z.; Joseph, J. G.; Liu, S. X.; Cheung, M. K.; Haffey, P. J.; Kurabayashi, K.; Fu, J. Centrifugal Microfluidics for Sorting Immune Cells from Whole Blood. *Sens. Actuators, B* **2017**, *245*, 1050−1061.

(18) Pommer, M. S.; Zhang, Y.; Keerthi, N.; Chen, D.; Thomson, J. A.; Meinhart, C. D.; Soh, H. T. Dielectrophoretic Separation of Platelets from Diluted Whole Blood in Microfluidic Channels. *Electrophoresis* **2008**, *29*, 1213−1218.

(19) McGrath, J.; Jimenez, M.; Bridle, H. Deterministic Lateral Displacement for Particle Separation: A Review. *Lab Chip* **2014**, *14*, 4139−4158.

(20) Davis, J. A. Microfluidic Separation of Blood Components through Deterministic Lateral Displacement. *Ph.D. Thesis*, Princeton University, Princeton, NJ, 2008.

(21) Loutherback, K.; Chou, K. S.; Newman, J.; Puchalla, J.; Austin, R. H.; Sturm, J. C. Improved Performance of Deterministic Lateral Displacement Arrays with Triangular Posts. *Microfluid. Nanofluid.* **2010**, *9*, 1143−1149.

(22) Zeming, K. K.; Ranjan, S.; Zhang, Y. Rotational Separation of Non-Spherical Bioparticles Using I-Shaped Pillar Arrays in a Microfluidic Device. *Nat. Commun.* **2013**, *4*, 1625.

(23) Au, S. H.; Edd, J.; Stoddard, A. E.; Wong, K. H. K.; Fachin, F.; Maheswaran, S.; Haber, D. A.; Stott, S. L.; Kapur, R.; Toner, M. Microfluidic Isolation of Circulating Tumor Cell Clusters by Size and Asymmetry. *Sci. Rep.* **2017**, *7*, 2433.

(24) Inman, H. F.; Bradley, E. L. The Overlapping Coefficient as a Measure of Agreement between Probability Distributions and Point Estimation of the Overlap of Two Normal Densities. *Commun. Stat. - Theory Methods* **1989**, *18*, 3851−3874.

(25) Holm, S. H.; Beech, J. P.; Barrett, M. P.; Tegenfeldt, J. O. Simplifying Microfluidic Separation Devices towards Field-Detection of Blood Parasites. *Anal. Methods* **2016**, *8*, 3291−3300.

(26) Ranjan, S.; Zeming, K. K.; Jureen, R.; Fisher, D.; Zhang, Y. DLD Pillar Shape Design for Efficient Separation of Spherical and Non-Spherical Bioparticles. *Lab Chip* **2014**, *14*, 4250−4262.

(27) Zhang, Z.; Henry, E.; Gompper, G.; Fedosov, D. A. Behavior of Rigid and Deformable Particles in Deterministic Lateral Displacement Devices with Different Post Shapes. *J. Chem. Phys.* **2015**, *143*, 243145.

DOI: 10.1021/acsami.8b10513
ACS Appl. Mater. Interfaces 2018, 10, 34811−34816